



Contents lists available at ScienceDirect

Scripta Materialia

journal homepage: www.elsevier.com/locate/scriptamat

Synthesis of bioinspired ice-templated bulk metallic glass-alumina composites with intertwined dendritic structure

Je In Lee^{a,b,c}, Amy Wat^{d,e}, Jinyeon Kim^{a,f}, Chae Woo Ryu^a, Hye Jung Chang^f, Eun Soo Park^{a,*}, Robert O. Ritchie^{d,e,**}

^a Research Institute of Advanced Materials, Department of Materials Science and Engineering, Seoul National University, Seoul 08826, Republic of Korea

^b International Center for Young Scientists, National Institute for Materials Science, 1-2-1 Sengen, Tsukuba, Ibaraki 305-0047, Japan

^c Department of Materials Science and Engineering, Pusan National University, Busan 46241, Republic of Korea

^d Department of Materials Science and Engineering, University of California, Berkeley, CA 94720, USA

^e Materials Sciences Division, Lawrence Berkeley National Laboratory, Berkeley, CA 94720, USA

^f Advanced Analysis Center, Korea Institute of Science and Technology, Seoul 02455, Republic of Korea

ARTICLE INFO

Article history:

Received 1 May 2019

Received in revised form 15 July 2019

Accepted 16 July 2019

Available online xxxxx

Keywords:

Bulk metallic glass (BMG)

Composites

Infiltration

Intertwined dendritic structure

Mechanical properties

Data availability:

The data that support the finding of this study are available from Prof. Park (email: espark@snu.ac.kr) upon reasonable request.

ABSTRACT

We have successfully developed bulk-metallic glass (BMG) composites reinforced with intertwined dendritic alumina, inspired by the structure of nacre (Abalone shells). We harness the dendritic growth of ice crystals in a thermal gradient to assemble an alumina with dendritic pore architecture, which is then infiltrated with BMG-forming melt to make a bioinspired, micrometer-scale, intertwined BMG-alumina composite. The composite exhibits ultra-high strength with exceptional relative compressive strength, far better than ceramic particulate BMG composites. The method presented here can be further exploited to produce novel BMG composites with excellent mechanical properties.

© 2019 Acta Materialia Inc. Published by Elsevier Ltd. All rights reserved.

Bulk metallic glasses (BMGs) have been of significant interest as potential structural materials due to their high strength and large elastic strains, but their application has often been compromised by low tensile ductility due to limited plasticity, as plastic flow in many BMGs can result in a localized instability from the propagation of a single shear band [1]. Plasticity in BMGs can be enhanced, however, by introducing a second phase in the amorphous matrix to arrest the abrupt propagation of single shear bands; as such, this can promote the generation of multiple shear band formation during deformation [1–14]. In particular, significant tensile ductility with exceptional fracture toughness values have been demonstrated in the BMG composites with a dendritic second phase which was formed *in situ* during solidification [15]. However, these microstructural features were obtained for specific alloy compositions and processing conditions, which has limited systematic

investigation of the effects of reinforcement size, fraction and distribution on the mechanical properties of such materials.

From the perspective of processing BMG-ceramic composites, freeze-casting (ice-templating) represents an effective technique to synthesize anisotropic foam materials using ice to generate bioinspired “nacre-like” hierarchical architectures [16–18]. Porosity can be modified between 0 and 100% and lamellar morphology is tailorable at the micron-scale in the freeze-cast foams [16–19]. Indeed, the synthesis of various freeze-cast materials has stimulated widespread studies on the development of polymer-ceramic, metal-ceramic, and metal-metal composites with ice-templated reinforcements [20–22]. While conventional alloys like aluminum or copper have been utilized to infiltrate the freeze-cast foams and produce the composites, BMGs have been rarely used in the synthesis of the ice-templated composites [23].

In the current work, we demonstrate the development of an ice-templated BMG-alumina composite. A freeze-cast alumina is infiltrated with a Zr-based BMG-forming melt without any applied pressure, resulting from the excellent wettability of alumina by the BMG. The microstructures of the composites, prepared at various infiltration

* Corresponding author.

** Correspondence to: R.O. Ritchie, Department of Materials Science and Engineering, University of California, Berkeley, CA 94720, USA.

E-mail addresses: espark@snu.ac.kr (E.S. Park), roritchie@lbl.gov (R.O. Ritchie).

temperatures, are examined to show how the chemical reaction between the BMG-forming melt and alumina affects the interfacial bonding between the constituents. Furthermore, the mechanical properties of the composites are compared with other ceramic particulate BMG composites to evaluate their comparative properties and the general attributes of ice-templated BMG composites with intertwined dendritic structures.

The $Zr_{46}Cu_{30.14}Ag_{8.36}Al_8Be_{7.5}$ (in at.%) BMG ingots were fabricated by arc melting a mixture of pure elements and a commercial $Cu_{77.3}Be_{22.7}$ alloy under a Ti-gettered Ar atmosphere, which were then cast into a copper mold. Alumina preforms with interconnected pore channels showing a dendritic pore morphology (Fig. 1a) were prepared by freeze-casting [23]. The freeze-cast alumina was infiltrated with the BMG-forming melt using a quartz tube with inner diameter of 5 mm (Fig. 1b). The tube, sealed *in vacuo*, was placed in an electric resistance furnace heated to 880–1000 °C for 3 min to melt the BMG, and was then tapped on the bottom to supply fresh BMG melt to a piece of the freeze-cast alumina (with dimensions $3 \times 3 \times 15$ mm). The alumina immersed in the melt was then held for 10 min in the heated furnace to ensure the complete infiltration of the dendritic pores, before being rapidly cooled by water quenching.

The wettability of alumina by the BMG-forming melt was evaluated using the sessile drop method [24]. The glass-transition temperature (T_g), crystallization-onset temperature (T_x) and the enthalpy of crystallization (ΔH_x) of the composites were determined by differential scanning calorimetry analysis (DSC; DSC 8500, Perkin Elmer) at a heating rate of $0.667 \text{ K} \cdot \text{s}^{-1}$. Microstructures were observed by optical, scanning electron (SEM; SU 70, Hitachi), and transmission electron microscopy (TEM; Tecnai F20, FEI), the latter involving energy dispersive spectroscopy (EDS). Specimens for the TEM analysis were prepared by focused ion beam processing (FIB; Helios Nano-Lab 600i, FEI). Vickers indents were made by applying 1 kgf load on the polished surface of the composites. Compression tests, performed on the composites on an Instron

5967 testing machine, were carried out with parallelepiped specimens (with dimensions $1 \times 1 \times 2$ mm) at a strain rate of 10^{-4} s^{-1} .

Fig. 1c shows an optical micrograph of the ice-templated BMG-alumina composites, prepared at 880 °C, which reveals an intertwined dendritic architecture with an alumina content of about 40 vol%. The thickness of constituent phases was evaluated to be 13.3 and 7.7 μm for BMG (image in white) and alumina (image in black), respectively. It should be noted that without applied pressure, infiltration at temperatures below 880 °C was incomplete.

To understand how the freeze-cast alumina could be infiltrated with the Zr-based BMG-forming melt above 880 °C, the sessile drop images of the melt dropped onto an alumina substrate and on the alumina preform were analyzed to evaluate the wettability of the alumina (Fig. 1d–f). The BMG melt at 1000 °C spread on the alumina substrate and exhibited a contact angle (θ) of about 6° within 10 s (Fig. 1d). The low θ represents the high work of adhesion ($w = \gamma \cos\theta$, where γ is surface tension of a melt [25]), indicating high bonding strength between the melt and alumina. Fig. 1e shows the BMG melt dropped on the freeze-cast alumina at 920 °C, where the pore structure was aligned to the melt dispenser. Interestingly, the alumina with micron-scale dendritic pores was instantly infiltrated with the droplet within 1 s. The capillary pressure induced on the BMG melt was calculated to be about 0.4 MPa ($\Delta P = 4\gamma \cos\theta / D_e$, where D_e is the equivalent diameter of pores in the freeze-cast alumina [23]), which is similar to the external pressure required to fabricate particulate or fibrous Zr-based BMG composites [2–4]. These results indicate that the spontaneous infiltration of the freeze-cast alumina with micron-scale dendritic pores can be attributed to the excellent wetting of alumina by the BMG (Fig. 1f).

Fig. 2a shows the DSC curves of the ice-templated BMG-alumina composites prepared at 880, 900, 950, and 1000 °C. While T_x of the composites (517 °C) was lower than that of the as-cast monolithic BMG (557 °C), the present composites showed a large supercooled liquid region ($\Delta T = T_x - T_g$) of 85 K, which implies that the thermal stability of the

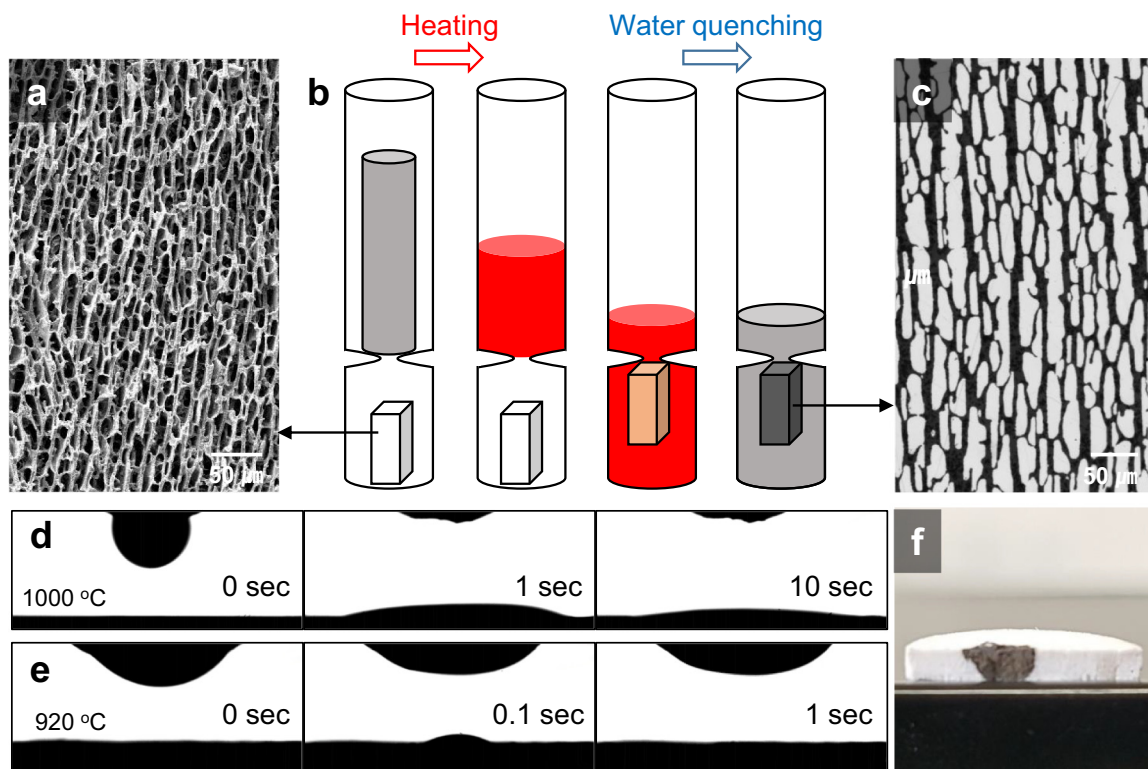


Fig. 1. (a) Microstructure of freeze-cast alumina with an alumina content of ~40 vol%. (b) Schematic of the pressureless melt-infiltration process. (c) Optical micrograph of an ice-templated BMG-alumina composite prepared at 880 °C. Representative sessile drop profiles on (d) an alumina substrate and (e) the freeze-cast alumina. (f) Cross-section of the freeze-cast alumina after the sessile-drop experiment shown in (e).

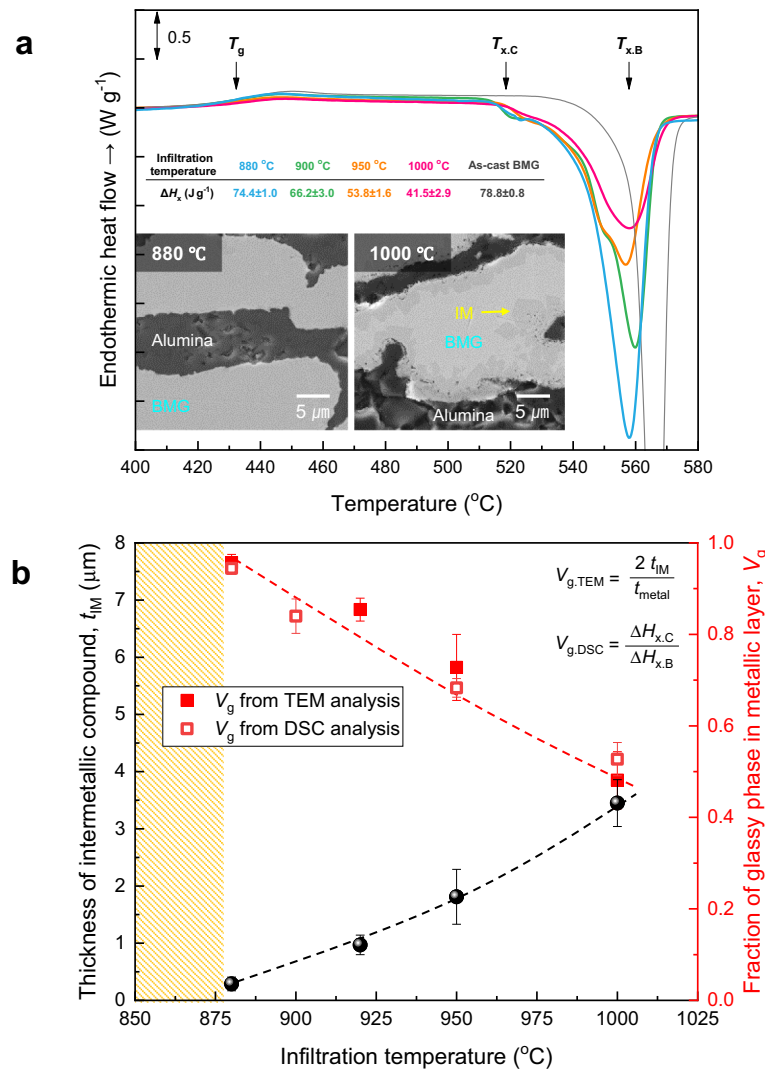


Fig. 2. (a) DSC traces of the ice-templated BMG-alumina composites depending on the infiltration temperatures. The SEM images (inset of (a)) show the metal-ceramic interfaces of the composites prepared at 880 and 1000 °C. (b) Thickness of the intermetallic compounds at the interface and fraction of glassy phase in the metallic layer for the composites depending on the infiltration temperatures.

glassy phase did not significantly deteriorate in the composites. In particular, ΔH_x of the composite prepared at 880 °C was 74.5 J·g⁻¹, which was ~95% of ΔH_x in the monolithic BMG (78.8 J·g⁻¹). However, with increasing infiltration temperature from 880 to 1000 °C, the ΔH_x of the composites continuously decreased to 41.5 J·g⁻¹. SEM imaging of the composite prepared at 1000 °C showed a faceted intermetallic compound with the average thickness of 3.4 μm at the interfaces, while the crystalline phase was not clearly seen in the SEM image of the composite prepared at 880 °C (inset in Fig. 2a).

Fig. 2b shows the thickness of the intermetallic compound, t_{IM} , in the ice-templated BMG-alumina composites prepared at 880, 920, 950, and 1000 °C. The value of t_{IM} was seen to gradually increase from 0.3 to 3.4 μm (Fig. 3a–d) as the infiltration temperature increased from 880 to 1000 °C. The fraction of the glassy phase in the metallic layer (V_g) was evaluated by microstructural analysis ($2t_{IM}/t_{metal}$, where t_{metal} is the thickness of the metallic phase); this indicated a decrease in V_g from 0.95 to 0.48 with an increase in the infiltration temperature from 880 to 1000 °C. The observed values of V_g agreed well with those calculated from thermal analysis ($\Delta H_{x,C}/\Delta H_{x,B}$, where subscripts C and B refer to composite and monolithic BMG, respectively). These results reveal that the decrease in V_g can be primarily attributed to the formation of intermetallic compounds at the interfaces. The increase in t_{IM} and the

decrease in V_g with increasing infiltration temperature are associated with the chemical reaction between the BMG melt and alumina [26], viz:



Since the formation of the ZrO₂ is accompanied by the dissolution of aluminum, this reaction results in a compositional shift from the initial alloy composition and thus a decrease in the glass-forming ability (GFA) of the melt.

Fig. 3a–d shows the TEM micrographs of the ice-templated BMG-alumina composites prepared at 880, 920, 950, and 1000 °C. All the composites exhibited the faceted intermetallic compound which was confirmed as the Zr₂Cu phase by x-ray diffraction (not shown) and selected area diffraction (inset in Fig. 3a) analyses. While the metal-ceramic interface appeared to be strongly bonded in the composite prepared at 880 °C, the composites prepared at 920, 950, and 1000 °C showed apparent cracks between the alumina and metallic layer. It can be understood that the crack caused by shrinkage occurring during crystallization was possibly intensified during FIB processing due to weaker interfacial bonding.

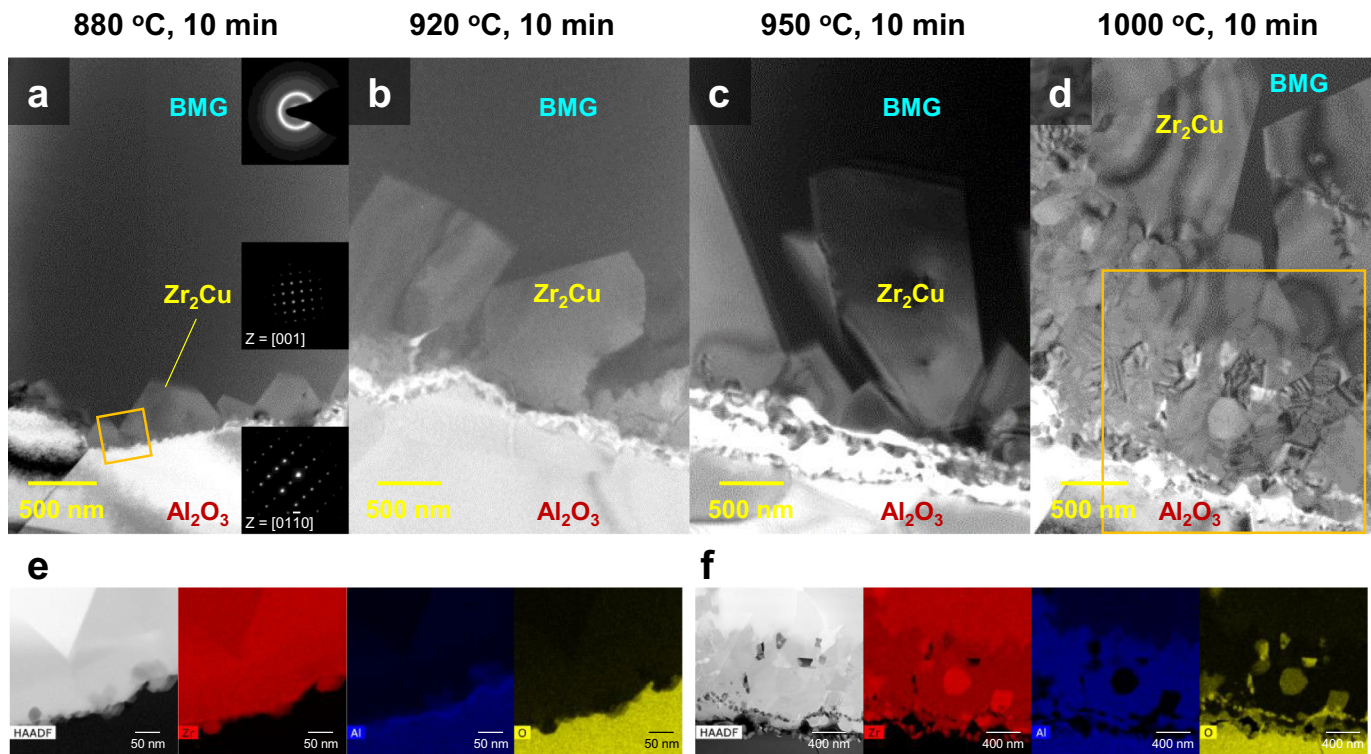


Fig. 3. BF-TEM micrographs of the ice-templated BMG-alumina composites prepared at (a) 880, (b) 920, (c) 950, and (d) 1000 °C. The inset of (a) shows selected area diffraction patterns of the glassy, Zr_2Cu , and alumina phases. HAADF images and EDS elemental maps of Zr, Al, and O for the composites prepared at (e) 880 and (f) 1000 °C (marked by the orange boxes in a and d, respectively). (For interpretation of the references to color in this figure legend, the reader is referred to the web version of this article.)

Fig. 3e–f shows the EDS elemental maps at the interfaces in Fig. 3a, d (marked by the orange boxes). The composite prepared at 880 °C showed spherical-shaped particles with the average size of 30 nm at the interface, which were depleted in oxygen but enriched in Zr and Al. The composite prepared at 1000 °C (Fig. 3f) showed that the ~1.5- μ m thick intermediate layer between the crack and Zr_2Cu phase was enriched in Al. EDS analysis revealed that the Al/Zr concentration ratio of the intermediate layer was about 1.3, which was much higher than the ratio of the glassy phase (0.17). Furthermore, the ZrO_2 phase, enriched in Zr and O (Fig. 3f), was found in the intermediate layer (average size of 200 nm) and on the alumina (average size of 45 nm). These results reveal that the reaction shown by Eq. (1) was more favorable at 1000 °C, leading to the local enrichment of Al at the interface and thus a decrease in the GFA of the BMG-forming melt. Furthermore, the formation of ZrO_2 on the alumina also leads to weak interfacial bonding since the wettability of ZrO_2 by Zr-based BMGs significantly deteriorates as the temperature increases from 880 to 1000 °C [27]. The ZrO_2 was barely observed and the amount of the Al-rich intermetallic compound was small in the composite prepared at 880 °C, implying that the chemical reaction can be suppressed by lowering infiltration temperature, thereby leading to strong interfacial bonding.

Fig. 4a shows the compressive stress-strain curves of the monolithic BMG, freeze-cast alumina and ice-templated BMG-alumina composites prepared at 880 and 1000 °C, where the dendritic structure was aligned to the compressive loading direction. The freeze-cast alumina containing 60 vol% dendritic pores showed compressive strength (σ_f) of 75 ± 5 MPa which is over 30 times lower than dense alumina (>2500 MPa [28]). Interestingly, the composite prepared at 880 °C exhibited a high σ_f of 2490 ± 65 MPa which is almost 40% higher than that of the monolithic BMG (1818 ± 53 MPa), although the composite prepared at 1000 °C exhibited relatively low σ_f of 403 ± 35 MPa. These results imply that the mechanical properties of the ice-templated composites were significantly affected by interfacial structure (Fig. 3).

Following the compression tests, the composite prepared at 880 °C exhibited shear fracture surfaces with vein patterns in the metallic layer (Fig. 4b), indicating local heating of the BMG due to significant energy release during fracture [29]. However, the composite prepared at 1000 °C fractured in a splitting mode and its fracture surface exhibited a microscopic roughness characteristic of freeze-cast alumina (Fig. 4c). SEM imaging of Vickers indents revealed that plastic flow had occurred in the BMG in the composite prepared at 880 °C, in the form of shear bands near the indent (Fig. 4d), while the composite prepared at 1000 °C exhibited cracks that had propagated in the vicinity of the interfaces (marked by arrows, Fig. 4e) where Zr_2Cu phase and intermediate layer formed (Fig. 3d, f). These results reveal that the composite prepared at 880 °C was reinforced with intertwined dendritic alumina due to strong interfacial bonding, whereas the strength of the composite prepared at 1000 °C deteriorated due to weak interfacial bonding and the brittle nature of the Zr_2Cu phase and intermediate layer.

The inset in Fig. 4a shows the relative compressive strength ($\sigma_{f,c}/\sigma_{f,b}$) of the ice-templated BMG-alumina composites compared against that of Zr- and Cu-based BMG composites reinforced with particulate ceramic materials [3,6–12]. The present composite prepared at 880 °C, reinforced with about 40 vol% alumina, exhibited $\sigma_{f,c}/\sigma_{f,b}$ of ~1.4 in proportion to alumina fraction; however, the ceramic particulate BMG composites showed a decrease in $\sigma_{f,c}/\sigma_{f,b}$ as the reinforcement fraction increased above 20 vol% due to the agglomeration of particles [10,12] or the decrease in V_g [9].

Since crystallization of the glassy phase occurred at metal-ceramic interfaces due to heterogeneous nucleation and chemical reaction (Fig. 3), mechanical properties of BMG composites are affected by the total area of the interfaces. For a particulate composite, the area of matrix-reinforcement interfaces per unit volume (A_p) can be expressed as below [30];

$$A_p = \frac{6V_p}{d}, \quad (2)$$

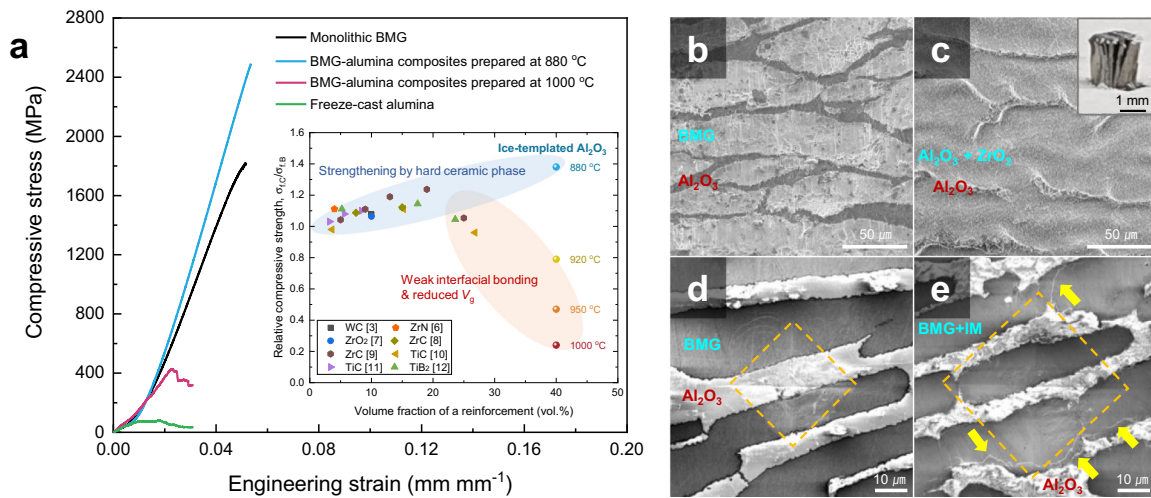


Fig. 4. (a) Compressive stress-strain curves of the monolithic BMG, freeze-cast alumina, and ice-templated BMG-alumina composites prepared at 880 and 1000 °C. The inset in (a) shows the relative compressive strength of the present composites compared with various Cu- and Zr-based BMG composites reinforced with particulate ceramic materials [3,6–12]. SEM images of fracture surfaces for the composites prepared at (b) 880 and (c) 1000 °C. The inset in (c) shows an image of the specimen after a compressive test. SEM images of Vickers indents for the composites prepared at (d) 880 and (e) 1000 °C.

where V_p and d are the fraction and diameter of the particles, respectively. Assuming the same alumina fraction and size as the present composites, the volume fraction of interfacial compounds ($V_{IM} = 100 \times A_p t_{IM}$, [31]) for a particulate BMG composite can be estimated. If t_{IM} is assumed to be 0.3 μm , V_{IM} is calculated to be ~9.4 vol%, which is more than three times higher than the experimentally measured V_{IM} ($100 \times (1 - V_p)(1 - V_g)$, 3 vol%) in the ice-templated composite prepared at 880 °C. This result reveals that an intertwined composite shows a much smaller A_p and lower V_{IM} than a particulate composite; therefore, the crystallization of glassy phase can be suppressed and strong interfacial bonding can be achieved in intertwined BMG composites. Furthermore, ice-templated BMG-alumina composites can be made with a wide variation in alumina content, from 30 to 80 vol% (Fig. S1 in the Supplementary materials); moreover, the lamellar morphology of the freeze-cast materials can be modified at the micron-scale [16]. Accordingly, intertwined BMG composites can be produced with a high fraction and homogeneous distribution of a reinforcement, which leads to the significant improvement in mechanical properties (Fig. 4a).

The intertwined dendritic structure of the ice-templated BMG-alumina composite offers no direct path for cracks to propagate perpendicular to the loading axis, which serves to suppress brittle fracture in the BMG. Although the present ice-templated BMG-alumina composites showed lack of plasticity in compression, the ductility of ice-templated BMG composites may be enhanced by the infiltration of freeze-cast metals such as Mo [32] or W [18], which have been considered as a ductile reinforcement for BMGs [2,13]. However, the best means to optimize the microstructure to improve both strength and ductility in these composites is still unclear, and consequently merits further investigation.

In conclusion, we have successfully fabricated a BMG-alumina composite with intertwined dendritic structure through ice-templating technique and pressureless infiltration. Interestingly, we demonstrate that the ice-templated alumina reinforced BMG composites show a significant increase in compressive strength with exceptional relative compressive strength, far better than ceramic particulate BMG composites. In this work, we have used ice-templated BMG-alumina composite as a testbed but the concept that we have introduced is applicable to a wide range of BMGs and ceramics. The use of freeze casting to form a dendritic second phase is not limited to conventional ceramics, but can be easily extended to light-weight metals and even refractory metals. Indeed,

this strategy for designing ice-templated BMG composites may provide new pathways for the development of advanced hybrid materials with excellent mechanical properties.

Supplementary data to this article can be found online at <https://doi.org/10.1016/j.scriptamat.2019.07.023>.

Acknowledgements

This work was supported by the National Research Foundation of Korea (NRF) grant funded by the Korean government (Ministry of Science, ICT and Future Planning) (No. NRF-2018M3A7B8060601). A.W. and R.O.R. were supported by the U.S. Department of Energy, Office of Science, Office of Basic Energy Sciences, Division of Materials Sciences and Engineering under contract no. DE-AC02-05-CH11231. One of the authors (E.S.P.) also benefited from Institute of Engineering Research at Seoul National University. The authors gratefully acknowledge the sessile drop testing with Dr. J. Schmitz and Dr. A. Meyer (DLR, Germany).

References

- [1] J. Qiao, H. Jia, P. Liaw, *Mater. Sci. Eng. R* 100 (2016) 1–69.
- [2] H. Choi-Yim, R. Conner, F. Szuets, W.L. Johnson, *Acta Mater.* 50 (10) (2002) 2737–2745.
- [3] H. Choi-Yim, R. Busch, U. Köster, W. Johnson, *Acta Mater.* 47 (8) (1999) 2455–2462.
- [4] H. Choi-Yim, W.L. Johnson, *Appl. Phys. Lett.* 71 (26) (1997) 3808–3810.
- [5] J.I. Lee, S.Y. Kim, E.S. Park, *Intermetallics* 91 (2017) 70–77.
- [6] M. Hasegawa, D. Nagata, T. Wada, A. Inoue, *Acta Mater.* 54 (12) (2006) 3221–3226.
- [7] G. Xie, D.V. Louzguine-Luzgin, H. Kimura, A. Inoue, *Mater. Trans.* 48 (7) (2007) 1600–1604.
- [8] H. Kato, T. Hirano, A. Matsuo, Y. Kawamura, A. Inoue, *Scr. Mater.* 43 (6) (2000) 503–507.
- [9] T. Liu, P. Shen, F. Qiu, T. Zhang, Q. Jiang, *Adv. Eng. Mater.* 11 (5) (2009) 392–398.
- [10] H. Fu, H. Zhang, H. Wang, Q. Zhang, Z. Hu, *Scr. Mater.* 52 (7) (2005) 669–673.
- [11] T. Liu, P. Shen, F. Qiu, Z. Yin, Q. Lin, Q. Jiang, T. Zhang, *Scr. Mater.* 60 (2) (2009) 84–87.
- [12] H. Fu, H. Wang, H. Zhang, Z. Hu, *Scr. Mater.* 54 (11) (2006) 1961–1966.
- [13] H. Zhang, H. Li, A. Wang, H. Fu, B. Ding, Z. Hu, *Intermetallics* 17 (12) (2009) 1070–1077.
- [14] Y. Sun, H. Zhang, A. Wang, H. Fu, Z. Hu, C. Wen, P. Hodgson, *Appl. Phys. Lett.* 95 (17) (2009), 171910.
- [15] D.C. Hofmann, J.-Y. Suh, A. Wiest, G. Duan, M.-L. Lind, M.D. Demetriou, W.L. Johnson, *Nature* 451 (7182) (2008) 1085–1089.
- [16] S. Deville, *Adv. Eng. Mater.* 10 (3) (2008) 155–169.
- [17] S. Deville, E. Saiz, A.P. Tomsia, *Acta Mater.* 55 (6) (2007) 1965–1974.
- [18] A. Röthlisberger, S. Häberli, R. Spolenak, D.C. Dunand, *J. Mater. Res.* 31 (6) (2016) 753–764.
- [19] S. Deville, *Scr. Mater.* 147 (2018) 119–124.

- [20] A. Röthlisberger, S. Häberli, F. Krogh, H. Galinski, D.C. Dunand, R. Spolenak, *Sci. Rep.* 9 (1) (2019) 476.
- [21] M.E. Launey, E. Munch, D. Alsem, H. Barth, E. Saiz, A.P. Tomsia, R.O. Ritchie, *Acta Mater.* 57 (10) (2009) 2919–2932.
- [22] M.E. Launey, E. Munch, D.H. Alsem, E. Saiz, A.P. Tomsia, R.O. Ritchie, *J. R. Soc. Interface* 7 (46) (2010) 741–753.
- [23] A. Wat, J.I. Lee, C.W. Ryu, B. Gludovatz, J.Y. Kim, A.P. Tomsia, T. Ishikawa, J. Schmitz, A. Meyer, M. Alfreider, E.S. Park, R.O. Ritchie, *Nat. Commun.* 10 (1) (2019) 961.
- [24] J. Schmitz, J. Brillo, I. Egry, *J. Mater. Sci.* 45 (8) (2010) 2144–2149.
- [25] E. Saiz, R.M. Cannon, A.P. Tomsia, *Annu. Rev. Mater. Res.* 38 (2008) 197–226.
- [26] P. Shen, X.-H. Zheng, Q.-L. Lin, D. Zhang, Q.-C. Jiang, *Metall. Mater. Trans. A* 40 (2) (2009) 444–449.
- [27] P. Shen, X. Zheng, F. Qiu, Q. Jiang, H. Liu, Z. Liu, *J. Am. Ceram. Soc.* 94 (7) (2011) 2162–2170.
- [28] C. San Marchi, M. Kouzeli, R. Rao, J. Lewis, D. Dunand, *Scr. Mater.* 49 (9) (2003) 861–866.
- [29] G. He, Z.F. Zhang, W. Loser, J. Eckert, L. Schultz, *Acta Mater.* 51 (8) (2003) 2383–2395.
- [30] K.K. Chawla, *Ceramic Matrix Composites*, Chapman & Hall, London, 1993 164.
- [31] Z.R. Xu, K.K. Chawla, R. Mitra, M.E. Fine, *Scr. Mater.* 31 (11) (1994) 1525–1530.
- [32] S.-T. Oh, Y.D. Kim, M.-J. Suk, *Mater. Lett.* 139 (2015) 268–270.